LETTER

doi:10.1038/nature24670

An electric-eel-inspired soft power source from stacked hydrogels

Thomas B. H. Schroeder[1,2]*, Anirvan Guha[2]*, Aaron Lamoureux[3], Gloria VanRenterghem[3], David Sept[4,5], Max Shtein[3], Jerry Yang[6] & Michael Mayer[2,4]

Progress towards the integration of technology into living organisms requires electrical power sources that are biocompatible, mechanically flexible, and able to harness the chemical energy available inside biological systems. Conventional batteries were not designed with these criteria in mind. The electric organ of the knifefish *Electrophorus electricus* (commonly known as the electric eel) is, however, an example of an electrical power source that operates within biological constraints while featuring power characteristics that include peak potential differences of 600 volts and currents of 1 ampere[1,2]. Here we introduce an electric-eel-inspired power concept that uses gradients of ions between miniature polyacrylamide hydrogel compartments bounded by a repeating sequence of cation- and anion-selective hydrogel membranes. The system uses a scalable stacking or folding geometry that generates 110 volts at open circuit or 27 milliwatts per square metre per gel cell upon simultaneous, self-registered mechanical contact activation of thousands of gel compartments in series while circumventing power dissipation before contact. Unlike typical batteries, these systems are soft, flexible, transparent, and potentially biocompatible. These characteristics suggest that artificial electric organs could be used to power next-generation implant materials such as pacemakers, implantable sensors, or prosthetic devices in hybrids of living and non-living systems[3–6].

The ability to generate external electrical discharges from excitable cells has evolved independently at least six times in natural history[1,7]. In particular, the electric eel *Electrophorus electricus* is a system optimized by natural selection for power generation from ionic gradients[8,9]; its specialized electric organs can generate discharges of 100 W entirely from the flux of small ions[10]. The eel uses the resulting transient current spikes to defend itself as well as to detect and incapacitate prey[2,8]. From the point of view of engineering an electrical power source for operation within a living organism[9], the electric organ of *Electrophorus* provides a fascinating example of specialized anatomy and physiology (Fig. 1a, b), using thousands of membranes with densely packed, highly selective and actuatable ion channels to generate large voltages and currents[1,2] (Extended Data Table 1).

Inspired by *Electrophorus*, we have engineered a potentially biocompatible artificial electric organ using durable and accessible components as well as automated and scalable fabrication processes. This artificial electric organ is capable of generating potential differences in excess of 100 V by implementing three unique features of the electric organs of *Electrophorus*.

The first of these evolved features in the eel's electric organ is the arrangement of thousands of ion gradients in series by growing long and thin electrically active cells known as electrocytes in parallel stacks spanning the rear 80% of the eel's body[11] (Fig. 1a, b). The anterior and posterior membranes of electrocytes are bound, top and bottom, by insulating connective tissue, and function as separate membranes with selectivity for two different ions such that the transcellular potentials across both membranes add up in series[1,2,12]. Figure 1b illustrates the mechanism of generating potential differences and electrical discharges in a resting and firing electrocyte: in the resting state, the anterior and posterior membrane potentials cancel each other out. By contrast, during an impulse, the posterior membrane depolarizes to produce a total transcellular potential of approximately 150 mV (Fig. 1b). Large electric eels stack thousands of electrocytes in series and can generate potential differences of over 600 V (ref. 2); parallel arrangement of multiple stacks enables peak currents that approach 1 A at short circuit[8,13].

To generate an artificial electric organ, we mimicked the anatomy of the eel by using four compositions of hydrogel as analogues of the four major components of an electrocyte, namely, its membranes with differing ion selectivities on the anterior and posterior sides and its intracellular and extracellular salt compartments (Fig. 1b, Extended Data Fig. 1, Supplementary Information 1). Figure 1c, d illustrates that, upon initiation of registered contact, tetrameric repeating units of a high-salinity hydrogel, a cation-selective gel, a low-salinity gel, and an anion-selective gel in sequence formed ionically conductive pathways, establishing electrolyte gradients across tens to thousands of selectively permeable compartments. Using the principle of reverse electrodialysis[14], each of these 'tetrameric gel cells' generated 130–185 mV at open circuit (Fig. 1d), a value comparable to the potential generated by a single electrocyte[2]. Figure 2e, f illustrates that the potential differences arising from 2,449 gels stacked in series added linearly to reach 110 V.

The second evolved feature in the electric organs of *Electrophorus* ensures simultaneous excitation of electrocytes along the entire organ, which can exceed one metre in length. As nerve signals do not travel fast enough to activate all electrocytes simultaneously within the duration of a discharge (around 2 ms), *Electrophorus* ensures synchronous signal delivery by slowing down the arrival of neural impulses to the parts of the organ closest to the command nucleus[1].

The artificial electric organ also requires simultaneous activation across many gels to circumvent energy dissipation (Extended Data Fig. 2, Supplementary Information 2). Figure 2 shows two assembly strategies of an artificial electric organ, one based on fluidics and the other based on surface printing. The fluidic implementation automatically generated and positioned a series of gels sequentially using a programmable fluid dispenser (Supplementary Video 1). In this configuration, we prepared artificial electric organs with a maximum of 41 gels (Fig. 2a), and demonstrated that three gel columns in parallel delivered the expected triple current and power (Fig. 2b, c, Extended Data Table 2). Automated fluidic assembly therefore makes it possible to fill devices in parallel and enables the formation of a bundled artificial organ, the

[1]Department of Chemical Engineering, University of Michigan, Ann Arbor, Michigan, USA. [2]Adolphe Merkle Institute, University of Fribourg, Fribourg, Switzerland. [3]Department of Materials Science and Engineering, University of Michigan, Ann Arbor, Michigan, USA. [4]Department of Biomedical Engineering, University of Michigan, Ann Arbor, Michigan, USA. [5]Center for Computational Medicine and Biology, University of Michigan, Ann Arbor, Michigan, USA. [6]Department of Chemistry and Biochemistry, University of California San Diego, La Jolla, California, USA.
*These authors contributed equally to this work.

© 2017 Macmillan Publishers Limited, part of Springer Nature. All rights reserved.

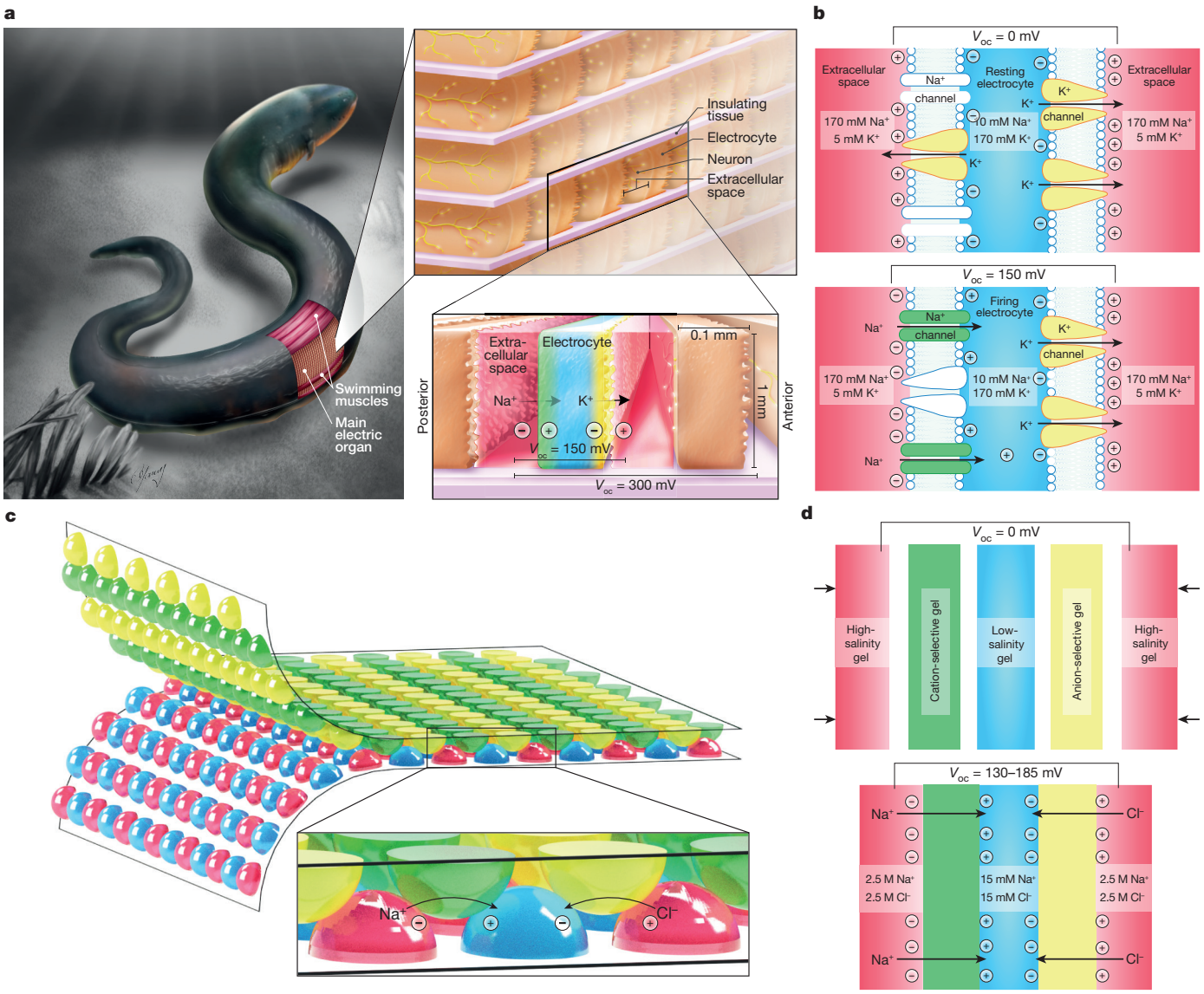

Figure 1 | Morphology and mechanism of action of the eel's electric organ and the artificial electric organ. a, *Electrophorus electricus*. The top inset shows the arrangement of electrocytes within the electric organs of *Electrophorus electricus*. The bottom inset shows ion fluxes in the firing state. V_{OC}, open-circuit voltage. **b**, Mechanism of voltage generation in electrocytes. The posterior membrane of each cell is innervated and densely packed with voltage-gated Na^+ channels; the anterior membrane is non-innervated and has papillar projections extending into the extracellular compartment that increase its surface area[2]. In the resting state, open K^+ channels in both membranes produce equal and opposite transmembrane potentials of −85 mV, so the total transcellular potential is zero (top). During an impulse, the Na^+ channels in the posterior membrane open and K^+ channels close in response to neural signals, generating an action potential of +65 mV from the resulting change in relative permeability to Na^+ and K^+ ions (Supplementary Information 1) and a total transcellular potential across both membranes of +150 mV (ref. 2) (bottom). **c**, Artificial electric organ in its printed implementation. In this and all subsequent figures, the red hydrogel was polymerized from neutral monomers and contains concentrated NaCl; the green gel was polymerized from negatively charged monomers and is cation-selective; the blue gel was polymerized from neutral monomers and contains dilute NaCl; and the yellow gel was polymerized from positively charged monomers and is anion-selective. **d**, Mechanism of voltage generation in the artificial electric organ. When gels are out of contact, no voltage is observed (top). Mechanical contact (bottom) brings together a sequence of gels such that ionic gradients are connected across alternating charge-selective membranes, producing potentials across each membrane that add up and can be stacked in series of thousands of gels (Supplementary Information 1). Images in **a**, **b** and **d** were printed with permission from Caitlin C. Monney.

current and power of which scale with the number of gel columns, analogous to the parallel electrocyte columns in the eel[1,2] (Fig. 2b, c). Although this first implementation of the fluidically assembled artificial electric organ required three seconds per gel plug, state-of-the-art microfluidics systems can generate water-in-oil droplets of four different compositions[15] at rates approaching 10^2 to 10^5 droplets per second[16], and ultraviolet-induced polymerization of hydrogel particles in a flow-through reactor has been demonstrated at a rate of 25 gelled particles per second[17]. At these rates, an artificial electric organ with 2,500 gels to generate 100 V could be assembled in less than two minutes. We demonstrated that by decoupling the fabrication from the assembly, for instance in the form of a tube pre-loaded with oil-separated hydrogel beads, assembly by pressure or external fields can be achieved within seconds (Supplementary Video 1).

As an alternative to this fluidic assembly strategy, Fig. 2d shows truly synchronous activation of an artificial electric organ by initiating mechanical contact between two complementary gel patterns over large arrays in a registered, parallel fashion. This design prints precursor solutions of ion-selective membranes in an array of lenses on one polyester substrate and precursor solutions of salt

© 2017 Macmillan Publishers Limited, part of Springer Nature. All rights reserved.

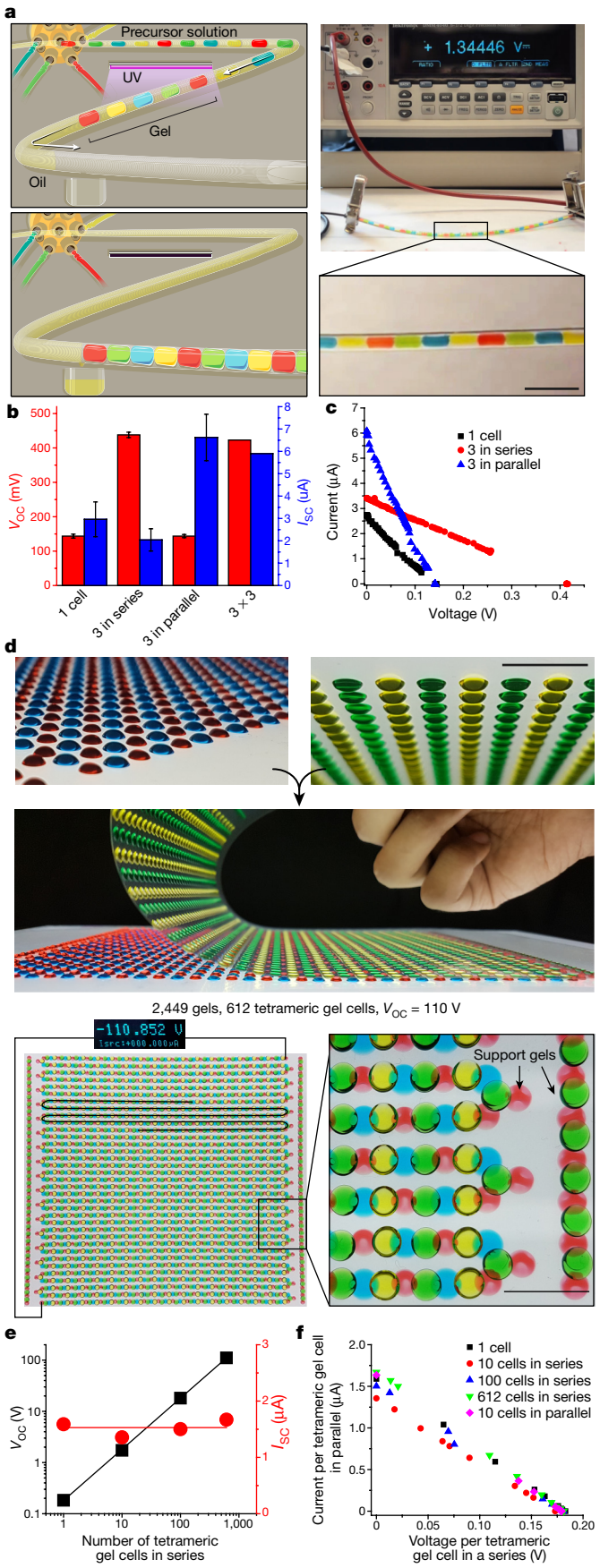

Figure 2 | Fluidic and printed artificial electric organs. a, The left panel shows a schematic of a fluidic artificial electric organ before (top) and after (bottom) contact activation. Aqueous plugs of hydrogel precursor solution were generated in mineral oil, cured with an ultraviolet (UV) lamp, and sequentially brought into mechanical contact after passing a small aperture in the tubing that allowed the interstitial oil to escape (Supplementary Video 1). The right panel shows a photograph of a fluidic artificial electric organ with ten tetrameric gel cells (inset; scale bar, 1 cm) generating 1.34 V. **b**, Open-circuit voltage and short-circuit current (I_{SC}) characteristics of a fluidic artificial electric organ. Open-circuit voltages (red bars) scale linearly when tetrameric gel cells are added in series; short-circuit currents (blue bars) scale linearly when tetrameric gel cells are added in parallel. (Error bars show s.d., $n = 3$, except for 3×3 in which $n = 1$). **c**, Plot of current and voltage in response to various external loads for one tetrameric gel cell (black squares), three cells in series (red circles), and three cells in parallel (blue triangles). **d**, Photographs of large complementary arrays of printed hydrogel lenses combining to form a continuous series of 2,449 gels with serpentine geometry. Support gels are used for mechanical stability and do not contribute to the system electrically. Scale bars, 1 cm. **e**, Open-circuit voltage and short-circuit current characteristics of printed artificial electric organs as a function of the number of tetrameric gel cells in a series. **f**, Normalized current–voltage relations of various numbers of tetrameric gel cells added in series or in parallel. The voltage axis is normalized by the number of cells in a series; the current axis is normalized by the number of tetrameric gel cells that are arranged in parallel. All points fall on one curve, as expected for a scalable system. Images in **a** were printed with permission from Caitlin C. Monney.

compartments on a second substrate in complementary patterns (Fig. 2d, Supplementary Video 2). When overlaid after curing, the resulting hydrogel lenses instantly form a serpentine ionically conductive pathway (Fig. 2d) with a repeating motif of potentials that add up to 110 V (Fig. 2e, f).

The third evolved feature in the electric organs of *Electrophorus* enables the maintenance and regeneration of large gradients of Na^+ and K^+ ions between the electrocyte cells and the extracellular space. ATP-dependent active transport by the Na^+/K^+-ATPase protein accomplishes this task by counteracting passive diffusion and rebuilding gradients after a discharge[2].

In the artificial electric organ, we achieved the maintenance of ionic gradients by ensuring physical separation between each of the hydrogels before actuation, with the benefit that this design did not require energy expenditure. We regenerated the artificial organ after discharge by applying a current to the terminal electrodes in a manner similar to that described previously[18], and recovered over 90% of the original capacity during at least ten discharges (Supplementary Information 3, Extended Data Fig. 3).

In terms of performance as a power source, the electric organs of *Electrophorus* can generate 600 V by stacking parallel columns of 100-μm-thick electrocytes with membrane contact areas[13] as large as 7,000 mm^2, minimizing the resistance of a layer of electrocytes to approximately 0.1 Ω (Table 1) and enabling discharges[10] of 100 W. By comparison, the 110-V implementation of the artificial electric organ involved a conductive pathway along thousands of relatively thick hydrogel lenses with a small cross-sectional contact area (Fig. 2d), increasing the resistance to 115 kΩ per tetrameric gel cell and limiting the power output to 50 μW across 2,449 gels (Fig. 2e, f, Supplementary Information 4).

To improve the performance, we devised flat hydrogel films on a patterned substrate and took advantage of a folding strategy that was originally developed to unfold solar panels in space (Fig. 3a, Extended Data Fig. 4, Supplementary Information 5). This *Miura-ori* fold makes it possible to stack a repeating series of thin films with a large contact area in a single synchronized and self-registered motion[19] (Supplementary Video 3). Table 1 shows that stacking 0.7-mm-thick films using an 80° *Miura-ori* fold yielded an artificial electric organ with a maximum power density of 27 ± 2 mW m^{-2} per tetrameric gel cell, owing to an approximately 40-fold reduction in resistance compared to lateral conduction through films of similar dimensions in the serpentine arrangement (Fig. 3b). As summarized in Table 1, the power density generated by this most efficient gel cell geometry is, however,

© 2017 Macmillan Publishers Limited, part of Springer Nature. All rights reserved.

Table 1 | Comparison of parameters from the natural and artificial electric organ

Source	Thickness of repeating unit* (m)	Cross-sectional area of electric organ (m^2)	Open-circuit voltage per repeating unit (V)	Internal resistance of repeating unit ($\Omega\ m^2$)	Maximum power density generated by repeating unit ($W\ m^{-2}$)
Live eels, anterior 6–10 cm of main organ (ref. 11)†	$(1.1\pm0.2)\times10^{-4}$	$(2.3\pm0.6)\times10^{-3}$	0.11 ± 0.01	$(6.8\pm0.7)\times10^{-4}$	5.5 ± 1.4
Live eels, sections of main organ (ref. 13)‡	10^{-4}	$(3.4\pm0.5)\times10^{-3}$	0.12 ± 0.01	$(5.1\pm0.4)\times10^{-4}$	10.6 ± 2.0
Live eels, leaping (ref. 8)§	10^{-4}	2.8×10^{-3}	0.16	4.8×10^{-4}	13.6
Gel cells, this work, 80° fold	2.8×10^{-3}	8.5×10^{-5}	0.17 ± 0.01	0.27 ± 0.02	0.027 ± 0.002

Where applicable, values are presented as mean ± s.e.m.
*Repeating unit refers to an electrocyte in the eel's electric organ (refs 8,11,13) and to a tetrameric gel cell in this work.
†Parameters are averages of the farthest anterior measurements for each of the four eels from table 2 of ref. 11. Cross-sectional area is estimated from eels of corresponding length in Table 1 of ref. 13.
‡Parameters are averages of all measurements from Table 1 of ref. 13. Repeating unit thickness is an estimate reported in ref. 13. Open-circuit voltage values were calculated by multiplying reported electromotive force values by a factor of 0.77 (an average factor reported in ref. 13). Unit resistance and power density were estimated for each eel based on the approximation made in ref. 13 that the external resistance was approximately equal to the internal resistance of the system.
§Average of two experiments. Open-circuit voltage and short-circuit current extracted from highest position attained by each ascending eel, for which both parameters are shown in figure 4c of ref. 8. Cross-sectional area estimated from eels of corresponding length in Table 1 of ref. 13, repeating unit thickness estimated from anterior voltage distributions reported in ref. 30. Assumptions: eel tilt angle, 70°; electric organ begins 20% of reported eel length from its front tip[11], resistance in the water tank from Fig. 3 of ref. 8 is negligible.

still 2–3 orders of magnitude smaller than the electrocyte layers in *Electrophorus*[12,13].

By bringing the design parameters of the artificial electric organ closer to those of the eel we may be able to improve its performance further. Electrocytes are thinner than the gel films shown in Fig. 3a by a factor of at least seven, and the absolute permeabilities of the ion-selective gel membranes used here were ten times smaller than the ion permeabilities of electrocyte membranes[20] (Extended Data Table 3). We showed that reducing the thickness of the hydrogel films by an order of magnitude increases the power density fivefold (Extended Data Fig. 5), and films of hydrogels as thin as a few hundred nanometres have been demonstrated in a different context[21]. Additionally, both the intracellular and extracellular compartments in the electric organs of *Electrophorus* are at a physiological ionic strength[12] of about 180 mM, imparting low resistivity, whereas the low-salinity compartment of the artificial electric organ contains only 15 mM sodium chloride and contributes most of the system's electrical resistance (Extended Data Fig. 5, Supplementary Information 6).

In this regard, the work here highlights a non-obvious strategy that the eel evolved to maximize power output. By developing electrocyte cells with two functionally different membranes such that, in the firing state, the posterior membrane is permeable specifically to sodium ions and the anterior membrane is permeable specifically to potassium ions (Fig. 1b), electrocytes convert the energy stored in opposing ion gradients of two different cations between physiological intracellular and extracellular solutions with low resistivity. By contrast, the broadly cation- or anion-selective hydrogel membranes in the artificial electric organ cannot distinguish between two different cations or anions, necessitating a gradient in overall ionic strength to establish a potential difference, and hence inherently requiring one compartment with lower ionic strength and considerably higher resistivity than the other (Supplementary Information 7). Therefore, the development of ultrathin synthetic membranes with improved ion selectivity[22] may increase the power density of artificial electric organs.

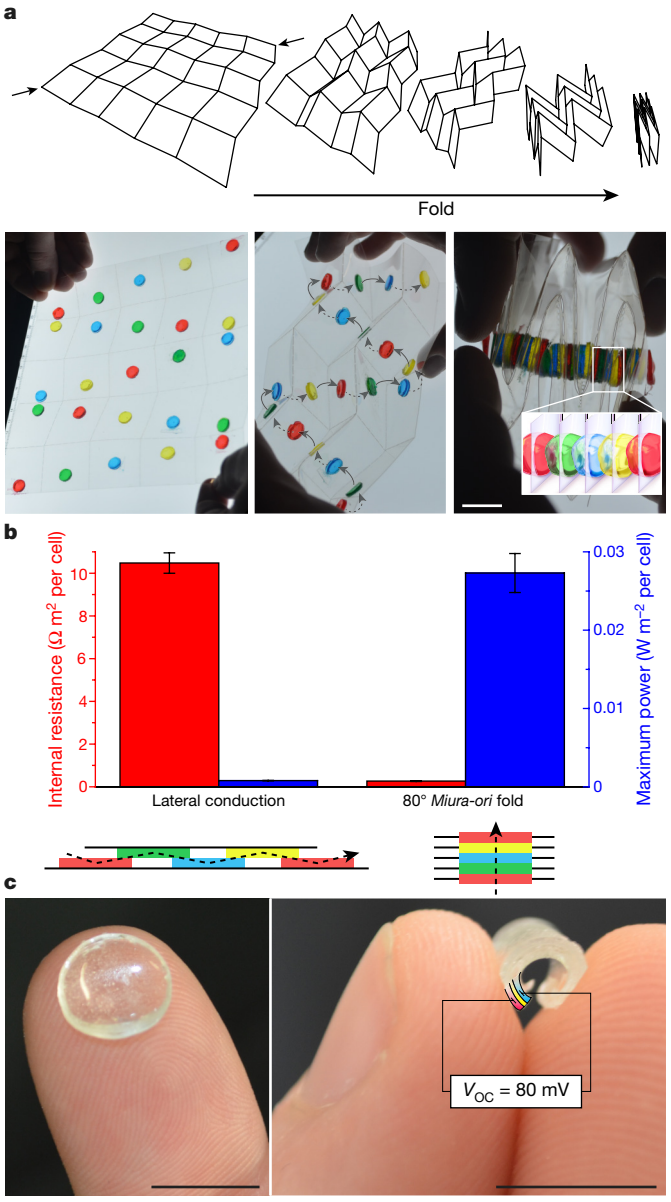

Figure 3 | Artificial electric organ morphologies based on thin hydrogel films. a, Schematic and photographs of *Miura-ori* folding. A single motion compresses a two-dimensional array of panels into a self-registered folded state where all panels overlap, generating a one-dimensional sequence[19]. This morphology was used to generate flat and relatively large contact areas between a series of thin gel films, which conducted ions from gel to gel through holes in the supporting polyester substrate. Scale bar, 1 cm. **b**, Area-normalized internal resistance (red) and maximum power (blue) per tetrameric gel cell with 0.7-mm-thick gel films arranged either laterally, in a manner that approximates the relative geometry of the serpentine implementation, or in a *Miura-ori*-assembled stack (error bars show s.e.m., $n = 3$; Supplementary Information 4). The stack geometry imparts a 40-fold reduction in resistance and a corresponding 40-fold improvement in maximum power output. **c**, Flexible and transparent artificial electric organ prototype with the shape of a contact lens (left). The prototype is composed of a gel trilayer of high-salinity gel (indicated by a false-coloured section in red), anion-selective gel (yellow), and low-salinity gel (blue) with a total thickness of 1.2 mm that produced an open-circuit voltage of 80 mV (right). Scale bars, 1 cm. Image in **a** was printed with permission from Caitlin C. Monney.

© 2017 Macmillan Publishers Limited, part of Springer Nature. All rights reserved.

Even before implementing these possible improvements, the unusual material properties of artificial electric organs may inspire opportunities that cannot be considered with conventional batteries. One example is the development of an electrically active contact lens made from hydrogel films. Contact lenses are usually fabricated from hydrogels, and prototypes with integrated displays and sensors have been reported[23,24]. To realize such functional lenses, an integrated and optically transparent power-harvesting scheme would be useful. Figure 3c illustrates a first step towards this vision. A single tri-layered lens generated a potential difference of 80 mV, suggesting the possibility of developing mouldable, flexible and optically transparent power sources for wearable and implantable devices[5,25]. Another example may be the use of artificial electric organs as deformable electric power sources in soft robots or other soft materials[26].

The work presented here introduces the implementation of an artificial electric organ from potentially biocompatible materials. By using thousands of compartmentalized ion gradients as well as scalable fabrication combined with synchronized assembly of ion-selective membranes, these materials are able to generate total open-circuit potential differences in excess of 100 V and power densities of 27 mW m^{-2} per tetrameric gel cell. Although these properties are only just approaching a useful power level for the lowest-power implant devices[27], advanced designs—possibly with thinner and more selective membranes—combined with strategies to recharge and activate[28] these artificial organs inside a living body[29] are likely to increase their utility. The eel's electric organ demonstrates that organic electrical power sources inside living organisms can operate with desirable power characteristics by using metabolically available energy. If next-generation designs can reduce the performance gap between the artificial and the natural electric organ by one or two orders of magnitude, then these artificial electric organs may open the door to metabolically sustained electrical energy for powering implants, wearables and other mobile devices.

Online Content Methods, along with any additional Extended Data display items and Source Data, are available in the online version of the paper; references unique to these sections appear only in the online paper.

Received 22 August; accepted 23 October 2017.

1. Bennett, M. V. L. in *Fish Physiology* Vol. 5 (eds Hoar, W. S. & Randall, D. J.) 347–491 (Academic Press, 1971).
2. Gotter, A. L., Kaetzel, M. A. & Dedman, J. R. *Electrophorus electricus* as a model system for the study of membrane excitability. *Comp. Biochem. Physiol. A Mol. Integr. Physiol.* **119,** 225–241 (1998).
3. Xu, J., Sigworth, F. J. & LaVan, D. A. Synthetic protocells to mimic and test cell function. *Adv. Mater.* **22,** 120–127 (2010).
4. Sun, H., Fu, X., Xie, S., Jiang, Y. & Peng, H. Electrochemical capacitors with high output voltages that mimic electric eels. *Adv. Mater.* **28,** 2070–2076 (2016).
5. Kim, D.-H. *et al.* Epidermal electronics. *Science* **333,** 838–843 (2011).
6. Whitesides, G. M. Assumptions: taking chemistry in new directions. *Angew. Chem. Int. Ed.* **43,** 3632–3641 (2004).
7. Gallant, J. R. *et al.* Nonhuman genetics. Genomic basis for the convergent evolution of electric organs. *Science* **344,** 1522–1525 (2014).
8. Catania, K. C. Leaping eels electrify threats, supporting Humboldt's account of a battle with horses. *Proc. Natl Acad. Sci. USA* **113,** 6979–6984 (2016).
9. Xu, J. & Lavan, D. A. Designing artificial cells to harness the biological ion concentration gradient. *Nat. Nanotechnol.* **3,** 666–670 (2008).
10. Brown, M. V. The electric discharge of the electric eel. *Electr. Eng.* **69,** 145–147 (1950).
11. Nachmansohn, D., Cox, R. T., Coates, C. W. & Machado, A. L. Action potential and enzyme activity in the electric organ of *Electrophorus electricus* (Linnaeus): I. Choline esterase and respiration. *J. Neurophysiol.* **5,** 499–515 (1942).
12. Keynes, R. D. & Martins-Ferreira, H. Membrane potentials in the electroplates of the electric eel. *J. Physiol*. **119,** 315–351 (1953).
13. Cox, R. T., Coates, C. W. & Brown, M. V. Electrical characteristics of electric tissue. *Ann. NY Acad. Sci*. **47,** 487–500 (1946).
14. Pattle, R. E. Production of electric power by mixing fresh and salt water in the hydroelectric pile. *Nature* **174,** 660–660 (1954).
15. Zeng, S., Li, B., Su, X., Qin, J. & Lin, B. Microvalve-actuated precise control of individual droplets in microfluidic devices. *Lab Chip* **9,** 1340–1343 (2009).
16. Bardin, D. *et al.* High-speed, clinical-scale microfluidic generation of stable phase-change droplets for gas embolotherapy. *Lab Chip* **11,** 3990–3998 (2011).
17. Young, C., Rozario, K., Serra, C., Poole-Warren, L. & Martens, P. Poly(vinyl alcohol)-heparin biosynthetic microspheres produced by microfluidics and ultraviolet photopolymerisation. *Biomicrofluidics* **7,** 44109 (2013).
18. Gumuscu, B. *et al.* Desalination by electrodialysis using a stack of patterned ion-selective hydrogels on a microfluidic device. *Adv. Funct. Mater.* **26,** 8685–8693 (2016).
19. Miura, K. *Method of Packaging and Deployment of Large Membranes in Space.* Report No. 618 (Institute of Space and Astronautical Science, 1985).
20. Shenkel, S. & Sigworth, F. J. Patch recordings from the electrocytes of *Electrophorus electricus*. Na currents and P_{Na}/P_K variability. *J. Gen. Physiol.* **97,** 1013–1041 (1991).
21. Ide, T., Takeuchi, Y. & Yanagida, T. Development of an experimental apparatus for simultaneous observation of optical and electrical signals from single ion channels. *Single Mol.* **3,** 33–42 (2002).
22. Feng, J. *et al.* Single-layer MoS_2 nanopores as nanopower generators. *Nature* **536,** 197–200 (2016).
23. Lingley, A. R. *et al.* A single-pixel wireless contact lens display. *J. Micromech. Microeng.* **21,** 125014 (2011).
24. Mansouri, K., Medeiros, F. A., Tafreshi, A. & Weinreb, R. N. Continuous 24-hour monitoring of intraocular pressure patterns with a contact lens sensor: safety, tolerability, and reproducibility in patients with glaucoma. *Arch. Ophthalmol.* **130,** 1534–1539 (2012).
25. Lai, Y.-C. *et al.* Electric eel-skin-inspired mechanically durable and super-stretchable nanogenerator for deformable power source and fully autonomous conformable electronic-skin applications. *Adv. Mater.* **28,** 10024–10032 (2016).
26. Ilievski, F., Mazzeo, A. D., Shepherd, R. F., Chen, X. & Whitesides, G. M. Soft robotics for chemists. *Angew. Chem. Int. Ed.* **50,** 1890–1895 (2011).
27. Chandrakasan, A. P., Verma, N. & Daly, D. C. Ultralow-power electronics for biomedical applications. *Annu. Rev. Biomed. Eng.* **10,** 247–274 (2008).
28. Enger, C. C. & Simeone, F. A. Biologically energized cardiac pacemaker: *in vivo* experience with dogs. *Nature* **218,** 180–181 (1968).
29. Chin, S. Y. *et al.* Additive manufacturing of hydrogel-based materials for next-generation implantable medical devices. *Sci. Robot.* **2,** eaah6451 (2017).
30. Cox, R. T., Rosenblith, W. A., Cutler, J. A., Mathews, R. S. & Coates, C. W. A comparison of some electrical and anatomical characteristics of the electric eel, *Electrophorus electricus*. *Zoologica* **25,** 553–562 (1940).

Supplementary Information is available in the online version of the paper.

Acknowledgements We are grateful to B. Rothen-Rutishauser and A. Petri-Fink at the Adolphe Merkle Institute for the use of their 3DDiscovery printer. F. Bircher's iPrint institute at the Haute École d'Ingénierie et d'Architecture Fribourg, particularly F. Bourguet and M. Soutrenon, donated time towards adapting a printer for our use and helped us to understand the intricacies of microvalve printing systems. Laser cutting was performed at Fablab Fribourg. U. Steiner's group, in particular P. Sutton and M. Fischer, provided instrumentation and advice related to impedance measurements. Research reported in this publication was supported by the Air Force Office of Scientific Research (grant FA9550-12-1-0435 to M.M., J.Y., D.S. and M.S.) and the National Institute of General Medical Sciences of the National Institutes of Health under award T32GM008353, which funds the Cellular Biotechnology Training Program (T.B.H.S.). The content is solely the responsibility of the authors and does not necessarily represent the official views of the National Institutes of Health.

Author Contributions T.B.H.S., A.G., J.Y. and M.M. conceived the project and designed the experiments. T.B.H.S. and A.G. performed all data collection. A.L. and M.S. provided the idea of *Miura-ori* folding. G.V. helped to define the parameters of the fluidic implementation. T.B.H.S. and D.S. conducted analysis of literature electrical datasets of *Electrophorus*. T.B.H.S., A.G. and M.M. wrote the manuscript.

Author Information Reprints and permissions information is available at www.nature.com/reprints. The authors declare no competing financial interests. Readers are welcome to comment on the online version of the paper. Publisher's note: Springer Nature remains neutral with regard to jurisdictional claims in published maps and institutional affiliations. Correspondence and requests for materials should be addressed to michael.mayer@unifr.ch.

Reviewer Information *Nature* thanks C. Bettinger, P. Calvert and A. Stokes for their contribution to the peer review of this work.

© 2017 Macmillan Publishers Limited, part of Springer Nature. All rights reserved.

METHODS

Materials and equipment. We purchased all chemicals from Sigma-Aldrich (Merck KGaA), except for 40% (w/v) 37.5:1 acrylamide/*N*,*N*′-methylenebisacrylamide (henceforth 'bis') solution (Bio-Rad) and P100 hydrophilic solution (Jonsman Innovation). We purified all water to 18.2 MΩ cm with a PURELAB Flex II purifier (ELGA LabWater, Veolia). We performed all fluidic gel handling with a FIAlab-3500 multi-analysis instrument (FIAlab Instruments Inc.) and an Infuse/Withdraw Pump 11 Elite programmable syringe pump (Harvard Apparatus) in Tygon tubing (1/16 inch inner diameter, 1/8 inch outer diameter, McMaster-Carr). We printed all patterns using a 3DDiscovery 3D bioprinter (regenHU) with a custom print plate machined at the University of Fribourg. The transparent substrates were A4-sized uncoated polyester overhead transparencies with a thickness of 0.1 mm (Avery Zweckform, 3555); we cut them using a Speedy 300 laser cutter (Trotec). We cured all gels using a Mineralight UV Display lamp (UVP, Analytik Jena) containing two 25-W, 302-nm or 365-nm UV tubes (Ushio Inc.).

Characterization of artificial electric organs. The first and final gel compartment of each series of gels was a high-salinity reservoir gel. We inserted Ag/AgCl wire electrodes into the first and final gel of each series, or in identical high-salinity reservoir gels that we brought into contact with the terminal gels. We recorded voltages using a Tektronix DMM4040 digital multimeter set to high input impedance mode and short-circuit currents using a Keithley 2400 SourceMeter using a source voltage of zero (except where noted). We constructed current–voltage curves (Fig. 2c, f) by connecting a series of known-load resistances to the batteries while monitoring the voltage across the load (Extended Data Fig. 6).

Fluidic artificial electric organ. The gel precursor solutions were all aqueous and had the following compositions: Low-salinity gel: 0.015 M sodium chloride, 0.045 M 2-hydroxy-4′-(2-hydroxyethoxy)-2-methylpropiophenone (henceforth 'photoinitiator'), 5.5 M acrylamide, 0.067 M bis. High-salinity gel: 0.5 M sodium chloride, 0.045 M photoinitiator, 5.4 M acrylamide, 0.066 M bis. Cation-selective gel: 2.0 M 2-acrylamido-2-methylpropane sulfonic acid, 0.014 M photoinitiator, 3.7 M acrylamide, 0.045 M bis. Anion-selective gel: 2.0 M (3-acrylamidopropyl) trimethylammonium chloride, 2.75 M acrylamide, 0.034 M bis. We used McCormick food dye to differentiate the gels during experiments.

We connected the inlets of the FIAlab multi-position valve to sources containing the four different gel precursor solutions, and to another containing mineral oil. A holding coil connected the main outlet of the valve to a syringe, which we used to withdraw liquids from the selected source into the holding coil. The main outlet was also connected to another source of mineral oil, which we pumped back through the outlet into a separate waste line to remove excess gel precursor. We programmed the FIAlab to withdraw a sequence of plugs of gel precursor solution ([high-salinity, cation-selective, low-salinity, anion-selective] × the number of repeats in the series), separating them with spacer plugs of mineral oil to prevent mixing of gels. After producing the desired number of plugs, we removed the collection tube and cured the gels under the ultraviolet lamp (365 nm) at a distance of 25 mm for 90 s. We connected the collection tube to a syringe filled with oil, then cut a notch-shaped opening on the opposite end of the tube, smaller than the thickness of the gel plugs. When we pushed the plugs past this notch, the interstitial oil escaped through the small opening and brought the entire sequence of gels into contact. We fabricated the first and final high-salinity gels separately and embedded the electrodes before curing. We connected these gels to the ends of the stacked gel sequence while applying light pressure, and clamped them into place before electrical characterization. Supplementary Video 1 illustrates the entire process.

Printed serpentine artificial electric organ for high voltages. The gel precursor solutions were aqueous and had the following compositions: Low-salinity gel: 0.015 M sodium chloride, 0.045 M photoinitiator, 4.1 M acrylamide, 0.051 M bis, 3.4 M glycerol. High-salinity gel: 2.5 M sodium chloride, 0.045 M photoinitiator, 5.1 M acrylamide, 0.062 M bis. Cation-selective gel: 2.0 M 3-sulfopropyl acrylate (potassium salt), 0.045 M photoinitiator, 1.9 M acrylamide, 0.055 M bis. Anion-selective gel: 2.0 M (3-acrylamidopropyl)trimethylammonium chloride, 2.75 M acrylamide, 0.034 M bis. Food dye from Städter was only used for photography and was absent during electrical recording experiments.

We printed two complementary arrays of 8 μL droplets of gel precursor solution on separate substrates in geometries that formed a single serpentine ionic pathway when overlaid (Fig. 2d). All the selective gel precursor droplets were printed onto the same substrate; the reservoir gel precursor droplets were printed onto the other one. After we finished printing onto a substrate, we immediately removed that substrate from the print plate and cured the gels under the ultraviolet lamp (302 nm) at a distance of 12 mm for 30 s. Once both substrates had been prepared, we overlaid them and applied a pressure of 16 kPa to the assembly to ensure contact between each of the gels in the series. In these experiments, voltages were collected with the SourceMeter using a source current of zero and currents were collected with a Keithley 6487 picoammeter.

80° *Miura-ori* folded artificial electric organ. The gel precursor solutions were the same as in the printed artificial electric organ. We laser-cut a 0.1-mm thick polyester substrate with perforations in the *Miura-ori* pattern (80°, short edge of the parallelogram = 4 cm; long edge = 4.06 cm) and one 7-mm diameter circular hole in each parallelogram positioned such that all the holes would overlap upon folding. We then attached polydimethylsiloxane (PDMS) pads with circular openings (depth = 0.3 mm, inner diameter = 10.5 mm) around each hole on both sides of the substrate, followed by manually pipetting the gel precursor solutions into each of the holes such that the PDMS reservoirs on both sides of the substrate were filled. We cured the solutions under an ultraviolet lamp (302 nm) at a distance of 12 mm for 30 s, then flipped the substrate over and cured the system for another 30 s. We peeled the PDMS reservoirs off the substrate before folding the substrates to bring the gels into contact (Fig. 3a). Painting a thin layer of deionized water onto both sides of each gel before folding prevented the gels from detaching from the substrate upon unfolding.

The power characteristics of the 80° *Miura-ori* folded geometry are compared with a lateral geometry of gels of the same dimensions as those shown in Fig. 3a. To make the lateral analogues, we attached PDMS pads with circular openings to two planar substrates (depth = 0.7 mm, inner diameter = 10.5 mm) with the rings on each substrate spaced 5 mm apart from one another to approximate the relative geometry of the serpentine implementation. We filled the openings on one substrate with alternating membrane precursor solutions and the openings on the other with alternating reservoir precursor solutions, then cured them with the same parameters as the 80° *Miura-ori* gels and registered them as with the serpentine geometry.

Gel trilayer in the shape of a contact lens. The gel precursor solutions were the same as in the printed artificial electric organ. We made thin reservoirs by mounting substrates above a block of Teflon with double-sided tape, pipetted the precursor solutions into the reservoirs, and cured them under an ultraviolet lamp (302 nm) at a distance of 12 mm for 30 s to form thin (0.4 mm) sheets of the low-salinity, high-salinity, and anion-selective gels. We assembled the gel films into a trilayer and used a biopsy punch to obtain a circular cutout (diameter = 10.5 mm).

Data availability. The data that support the findings of this study are available from the corresponding author upon reasonable request.

31. Schoffeniels, E. Ion movements studied with single isolated electroplax. *Ann. NY Acad. Sci.* **81,** 285–306 (1959).
32. Altamirano, M. & Coates, C. W. Effect of potassium on electroplax of *Electrophorus electricus*. *J. Cell. Comp. Physiol.* **49,** 69–101 (1957).
33. Nakamura, Y., Nakajima, S. & Grundfest, H. Analysis of spike electrogenesis and depolarizing K inactivation in electroplaques of *Electrophorus electricus*, L. *J. Gen. Physiol.* **49,** 321–349 (1965).

© 2017 Macmillan Publishers Limited, part of Springer Nature. All rights reserved.

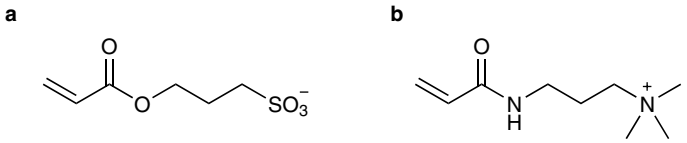

Extended Data Figure 1 | Charged monomers used in charge-selective 'membrane' gels. a, 3-Sulfopropyl acrylate, a component of the cation-selective gel. **b**, (3-Acrylamidopropyl)trimethylammonium, a component of the anion-selective gel.

© 2017 Macmillan Publishers Limited, part of Springer Nature. All rights reserved.

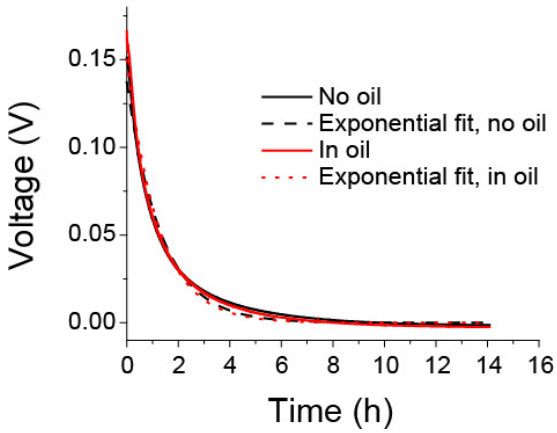

Extended Data Figure 2 | Self-discharge of artificial electric organ over time after contact between all gels, with and without exposure to ambient air. Curves were fit with a single exponential decay function (dotted curves); the half-time for each was 40 min. The artificial electric organ was assembled as described in Supplementary Information 3. Supplementary Video 1 shows a fluidic implementation of the artificial electric organ which positions gels into contact sequentially rather than simultaneously. Large-scale implementations of similar sequential positioning schemes may be prone to power loss from gradient depletion unless positioning could be accomplished rapidly.

© 2017 Macmillan Publishers Limited, part of Springer Nature. All rights reserved.

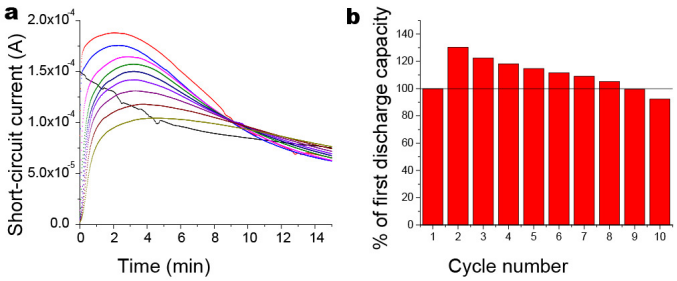

Extended Data Figure 3 | The artificial electric organ can be recharged. Experimental details in Supplementary Information 3. **a**, Current versus time recordings of ten discharges of a single tetrameric gel cell at short circuit following recharging. Initial discharge shown in black; subsequent discharges in the following order: red, blue, magenta, green, navy, purple, plum, wine, olive. **b**, Bar graph of normalized integrals of discharge curves.

© 2017 Macmillan Publishers Limited, part of Springer Nature. All rights reserved.

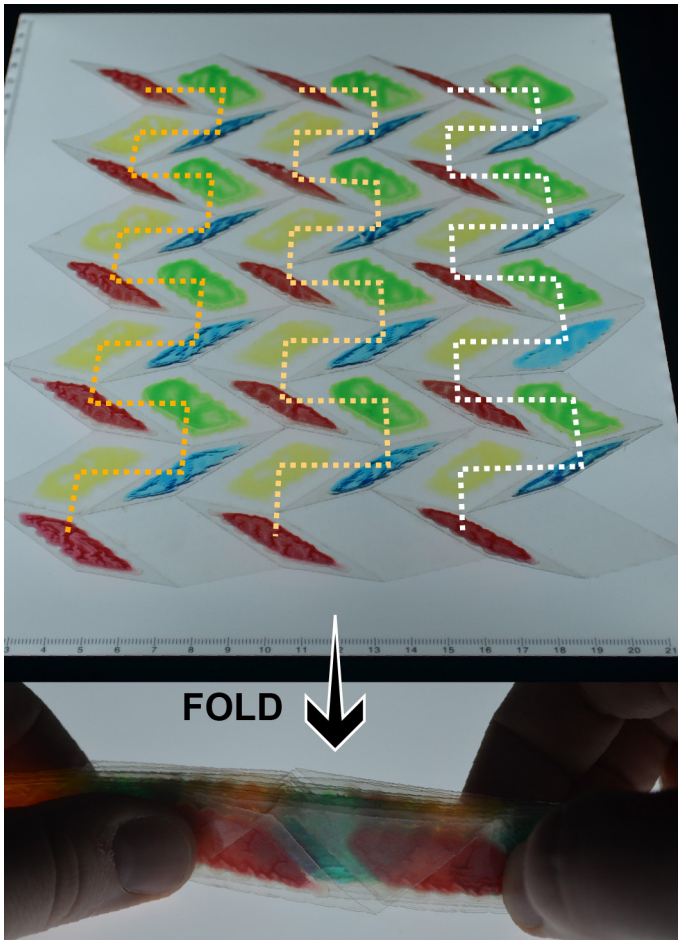

Extended Data Figure 4 | Geometrical arrangement of the printed 45° *Miura-ori* gel cells. Dotted lines of a single colour indicate gels forming a series. Different colours indicate parallel sequences. This fold geometry is scalable both in series for higher voltage output and in parallel for higher current. In contrast to the 80° *Miura-ori* fold, all gels are located on the same side of the substrate, facilitating fabrication by printing or other methods. (Supplementary Information 5).

© 2017 Macmillan Publishers Limited, part of Springer Nature. All rights reserved.

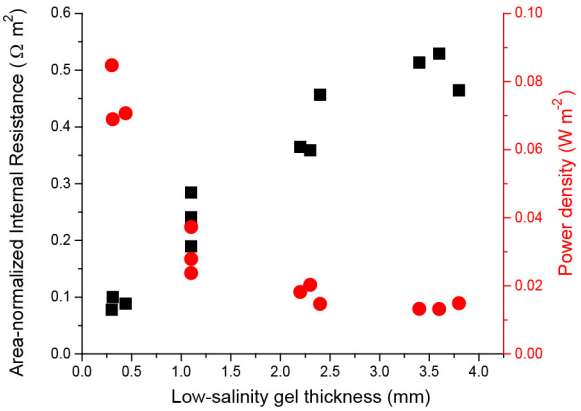

Extended Data Figure 5 | Internal resistance and power density of tetrameric gel cells as a function of thickness of low-salinity gel. Internal resistance, black squares; power density, red circles. The thicknesses of all other gels were held constant at 1 mm.

© 2017 Macmillan Publishers Limited, part of Springer Nature. All rights reserved.

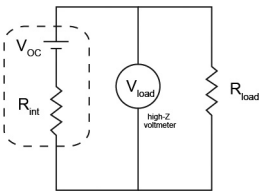

Extended Data Figure 6 | Equivalent circuit of an artificial electric organ connected to a load resistance. The elements within the dotted line represent the contribution of a single tetrameric gel cell; these can be added in series or in parallel. The impedance of the voltmeter that was used exceeded 10 GΩ; current through this pathway was assumed to be negligible.

© 2017 Macmillan Publishers Limited, part of Springer Nature. All rights reserved.

Extended Data Table 1 | Selectivity of membranes considered in this work

Reference	$[Na^+]_{in}$ (M)	$[Na^+]_{out}$ (M)	$[K^+]_{in}$ (M)	$[K^+]_{out}$ (M)	Membrane	V_{oc} (mV)	P_{Na}/P_K*	P_K/P_{Na}*
Keynes and Martins-Ferreira, 1953[12] †	0.01 [31]	0.172	0.17 [31]	0.005	Main organ, resting	-70.2 ± 2.9	.0354	28.3
					Main organ, peak	+55.1± 4.4	16.8	0.0597
					Sachs organ, resting	-78.1± 4.2	.0182	55.1
					Sachs organ, peak	+61.9 ± 2.1	31.3	0.0319
Altamirano and Coates, 1957[32] †	0.01 [31]	0.19	0.17 [31]	0.005	Sachs organ, resting	-84.0 ± 5.2	.00789	127
					Sachs organ, peak	+52.5 ± 2.6	11.7	0.0858
Nakamura *et al.*, 1965[33] †	0.01 [31]	0.172	0.17 [31]	0.005	Sachs organ, resting	-84.9 ± 2.7	.00366	140
					Sachs organ, peak	+52.3 ± 4.1	13.6	0.0734
Shenkel and Sigworth 1991[20]	0	0.2	0.2	0	Main organ, cell-attached patch, peak	+78.6 ± 6.7	21.3	0.0468
					Main organ, inside-out patch, peak	+72.7 ± 11	16.9	0.0590
					Sachs organ, cell-attached, peak	+78.6 ± 6.6	21.3	0.0468
					Sachs organ, inside-out patch, peak	+73.6 ± 4.1	17.6	0.0568
	$[Na^+]_{in}$ (M)	$[Na^+]_{out}$ (M)	$[Cl^-]_{in}$ (M)	$[Cl^-]_{out}$ (M)	Membrane	V_{oc} (mV)	P_{Na}/P_{Cl}	P_{Cl}/P_{Na}
This work	0.015	2.5	0.015	2.5	Anion-selective gel	-89.3 ± 0.6	0.0249 ± 0.0008	40.3 ±1.2
					Cation-selective gel	+82.3 ± 1.5	29.5 ± 1.9	0.0343 ± 0.0024

Electrocyte membranes listed here are all the posterior, innervated membranes; anterior membranes maintain resting potential over the duration of a discharge[12]. Permeability ratios calculated using Supplementary Equations (5) and (6). Where applicable, values are presented as mean ± s.e.m.

*Calculated from mean zero-current voltage.

†Interior concentration values not provided; taken from ref. 31.

© 2017 Macmillan Publishers Limited, part of Springer Nature. All rights reserved.

Extended Data Table 2 | Electrical characteristics from fluidic assembly of gel cells in series and parallel

Cell arrangement	V_{oc} (mV)	R_{int}/L^* (kΩ/mm)
One cell	143 ± 3	4.8 ± 0.8
Three cells in series	438 ± 5	14.6 ± 0.9
Three cells in parallel	143 ± 3	2.0 ± 0.1
Three series of three cells in parallel	423	4.6

Where applicable, values are presented as mean ± s.e.m.
*Internal resistance normalized by effective cell length, which accounts for differences in the extent of compression. $n = 3$ for all values except those in the final row.

© 2017 Macmillan Publishers Limited, part of Springer Nature. All rights reserved.

Extended Data Table 3 | Absolute permeability values of membranes considered in this work

Reference	$[Na^+]_{in}$ (M)	$[Na^+]_{out}$ (M)	$[K^+]_{in}$ (M)	$[K^+]_{out}$ (M)	Membrane	V_{oc} (mV)	P_{Na} (m s^{-1})	P_K (m s^{-1})
Shenkel and Sigworth 1991[20]*	0	0.2	0.2	0	Sachs organ inside-out patch, peak	+75.3 ± 2.4	(1.91 ± 0.28) x 10^{-7}	(8.74 ± 1.10) x 10^{-9}
	$[Na^+]_{in}$ (M)	$[Na^+]_{out}$ (M)	$[Cl^-]_{in}$ (M)	$[Cl^-]_{out}$ (M)	Membrane	V_{oc} (mV)	P_{Na} (m s^{-1})	P_{Cl} (m s^{-1})
This work	0.015	2.5	0.015	2.5	Anion-selective gel	-89.3 ± 0.6	(6.71 ± 4.10) x 10^{-10}	(2.61 ± 1.51) x10^{-8}
					Cation-selective gel	82.3 ± 1.5	(2.03 ± 0.33) x 10^{-8}	(7.44 ± 1.71) x10^{-10}

Where applicable, values are presented as mean ± s.e.m.
Permeabilities calculated using Supplementary Equations (3) and (8).
*Values calculated from reversal potential (E_r) and maximum current (I_{max}) values reported in Table 1 of ref. 20.
Assumptions: I_{max} occurs at +10 mV (reported average value) for all experiments; Ohmic behaviour between E_r and I_{max} (appears approximately correct based on the shape of the curve in figure 1b of ref. 20); Patch area of 10 μm^2 (assumed in discussion of ref. 20).
Comparisons of absolute permeabilities in the main text were made based on these permeability values from firing electrocytes.

© 2017 Macmillan Publishers Limited, part of Springer Nature. All rights reserved.